Pliocene Warmth, Polar Amplification, and Stepped Pleistocene Cooling Recorded in NE Arctic Russia

Julie Brigham-Grette *et al.*

Science **340**, 1421 (2013);
DOI: 10.1126/science.1233137

Pliocene Warmth, Polar Amplification, and Stepped Pleistocene Cooling Recorded in NE Arctic Russia

Julie Brigham-Grette,[1]* Martin Melles,[2] Pavel Minyuk,[3] Andrei Andreev,[2] Pavel Tarasov,[4] Robert DeConto,[1] Sebastian Koenig,[1] Norbert Nowaczyk,[5] Volker Wennrich,[2] Peter Rosén,[6] Eeva Haltia,[5]† Tim Cook,[7] Catalina Gebhardt,[8] Carsten Meyer-Jacob,[6] Jeff Snyder,[9] Ulrike Herzschuh[10]

Understanding the evolution of Arctic polar climate from the protracted warmth of the middle Pliocene into the earliest glacial cycles in the Northern Hemisphere has been hindered by the lack of continuous, highly resolved Arctic time series. Evidence from Lake El'gygytgyn, in northeast (NE) Arctic Russia, shows that 3.6 to 3.4 million years ago, summer temperatures were ~8°C warmer than today, when the partial pressure of CO_2 was ~400 parts per million. Multiproxy evidence suggests extreme warmth and polar amplification during the middle Pliocene, sudden stepped cooling events during the Pliocene-Pleistocene transition, and warmer than present Arctic summers until ~2.2 million years ago, after the onset of Northern Hemispheric glaciation. Our data are consistent with sea-level records and other proxies indicating that Arctic cooling was insufficient to support large-scale ice sheets until the early Pleistocene.

The geologic record makes it clear that global temperatures are intimately linked to changes in atmospheric greenhouse gas concentrations (*1*). Today's CO_2 levels are similar to Pliocene estimates [4.5 to 2.588 million years ago (Ma)], ranging from 380 to 450 parts per million (ppm), or some 30% higher than preindustrial levels (*2*, *3*). Pliocene warmth, considered an analog for future climate scenarios, persisted across repeated warm and cool Milankovitch cycles, raising questions concerning climate sensitivity to CO_2. Moreover, it remains unclear what mechanisms drove the amplification of polar temperatures and past reductions in sea ice (*4*, *5*) and the eventual cooling and growth of continental Northern Hemispheric ice sheets. The PRISM climate mapping program (*6*) compiled important global climate information for the interval from 3.26 to 3.02 Ma but overlooked the earlier middle Pliocene, millennial-scale variability of cooler Pliocene climate states, and the Pliocene/Pleistocene transition [boundary at 2.588 Ma (*7*)]. The terrestrial Arctic is rich in Pliocene stratigraphic sequences that document time slices when conditions were much warmer than today (*8*–*10*). Yet marine sediments on the Lomonosov Ridge suggest that the Arctic Ocean has maintained perennial sea ice (*11*–*13*) or perhaps periods of seasonal sea ice since the middle Miocene (*14*). The discordance between terrestrial and Arctic marine records has remained unresolved largely because of the lack of continuous land records for comparison (*15*, *16*).

Here we present results from a continuous, middle Pliocene to early Pleistocene lacustrine record from the terrestrial Arctic, derived from Lake El'gygytgyn, located 100 km north of the Arctic Circle in Chukotka, northeastern Russia (67°30'N, 172°05'E; Fig. 1). The basin was created by a meteorite impact 3.58 ± 0.04 Ma (*17*) and contains a continuous sediment sequence recording a complete Late Cenozoic climate history on centennial to millennial time scales. The data here demonstrate extreme warmth and polar amplification during the middle Pliocene, stepped cooling events during the Pliocene-Pleistocene transition, and the recurrence of Arctic summer warmth until after 2.2 Ma, after the paced onset of Northern Hemispheric glaciation (*3*, *18*, *19*). Recurring but declining warmth in the Arctic borderlands has implications for understanding the transition from a forested Arctic in the middle Pliocene to the tundra-dominated landscape of today. Moreover, the data raise questions concerning

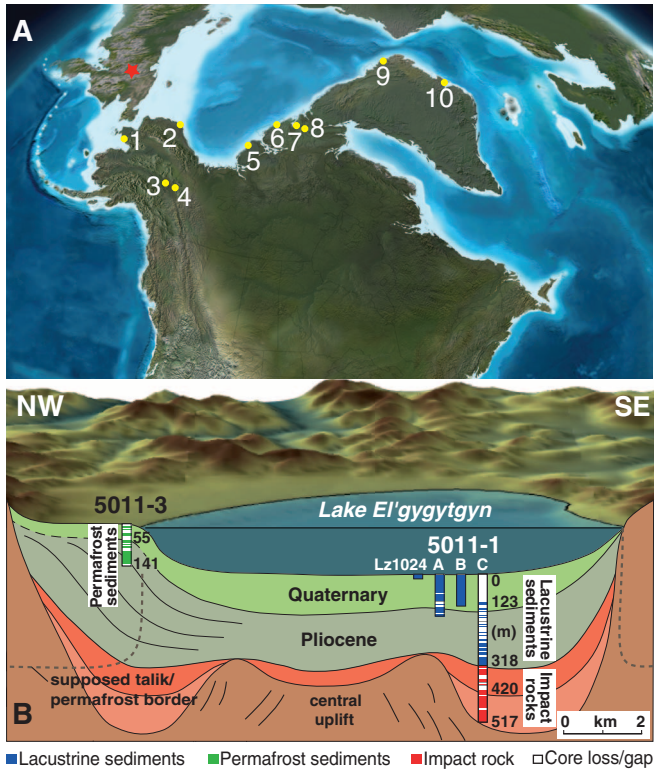

Fig. 1. Location of Lake El'gygytgyn and stratigraphic cross section. (**A**) Lake El´gygytgyn (star) formed 3.58 Ma in NE Russia, when North America remained a contiguous landmass (and had a more continental climate), unbroken by tectonics and glacially eroded marine troughs (*33*) (map courtesy of Ron Blakely). Selected Pliocene and early Pleistocene sites mentioned in the text and supplemental materials are shown (1, Nome; 2, Gubik Formation; 3, Klondike Area; 4, Lost Chicken; 5, Banks Island; 6, Hvitland Beds; 7, Meighen Island; 8, Strathcona Fjord; 9, Kap København; 10, Lodin Elv). (**B**) Schematic cross-section of the El´gygytgyn basin stratigraphy, showing the location of ICDP sites 5011-1 and 5011-3. At site 5011-1, three holes (1A, 1B, and 1C) were drilled to replicate the Quaternary and uppermost Pliocene sections. Hole 1C penetrated the remaining lacustrine sequence down to a depth of 318 m and then ~200 m into the impact rock sequence underneath. Lz1024 is a 16-m-long percussion piston core taken in 2003 that fills the stratigraphic gap between the lake sediment surface and the top of drill cores 1A and 1B (*18*).

[1]Department of Geosciences, University of Massachusetts, 611 North Pleasant Street, Amherst, MA 01003, USA. [2]Institute of Geology and Mineralogy, University of Cologne, Zuelpicher Strasse 49a, D-50674 Cologne, Germany. [3]North-East Interdisciplinary Scientific Research Institute, Far East Branch of the Russian Academy of Sciences, Portovaya Street 16, 685000 Magadan, Russia. [4]Free University Berlin, Institute of Geological Sciences, Malteser Strasse 74-100, Haus D, D-12249 Berlin, Germany. [5]Helmholtz Centre Potsdam, GFZ German Research Centre for Geosciences, Telegrafenberg, D-14473 Potsdam, Germany. [6]Department of Ecology and Environmental Science, Umeå University, SE-901 87 Umeå, Sweden. [7]Department of Physical and Earth Sciences, Worcester State University, Worcester, MA 01602, USA. [8]Alfred Wegener Institute for Polar and Marine Research, Am Handelshafen 12, D-27570 Bremerhaven, Germany. [9]Department of Geology, Bowling Green State University, OH 43403, USA. [10]Alfred Wegener Institute for Polar and Marine Research, Research Unit Potsdam, Telegrafenberg A43, D-14473 Potsdam, Germany.

*Corresponding author. E-mail: juliebg@geo.umass.edu
†Present address: Department of Geology, Lund University, Sölvegatan 12, S-223 62 Lund, Sweden.

the seasonal persistence of Arctic sea ice in the past, the evolution of Northern Hemisphere ice sheets, and the onset of major glacial-interglacial cycles (*20*, *21*).

Lake Setting, Core Acquisition, and Methods

At the time of the El′gygytgyn impact 3.6 Ma (*17*), the North American Arctic had a more continental geography (Fig. 1), forests reached the Arctic Ocean coast (*10*), Greenland was mostly ice-free (*22*, *23*), and permafrost was not widespread (*10*, *24*). Today Lake El'gygytgyn is 170 m deep and 12 km in diameter, with an area of 110 km^2 within a catchment of only 293 km^2 (*25*). It is cold, monomictic, and oligotrophic, with a summer temperature of ~3°C. Distinct lake-level changes are recorded by terraces and wave-cut notches as high as 35 to 40 m above and 10 m below the modern lake level, with the highest benches occurring in the early basin history (*26*, *27*).

The Lake El'gygytgyn region today has a mean annual air temperature (MAT) of –10°C, with mean July temperatures of ~+8°C and average winter lows of ~–35°C. Mean annual precipitation (PANN) is about 200 mm/year. Reanalysis data show that the climatology of the basin is representative of much of the western Arctic (*25*). Although the lake area currently lies within the subzone of southern shrub tundra, today's climatology supports only sparse vegetation, dominated by hummock and moss tundra over deep permafrost with some prostrate willows and dwarf birch.

Drilling at Lake El'gygytgyn occurred in spring 2009 from a lake-ice platform (*28*). Lake basin stratigraphy is based on seismic surveys (*29*) suggesting continuous sedimentation over the time period of interest. The 318-m-long composite sequence representing the complete 3.6 Ma record in International Continental Scientific Drilling Program (ICDP) core 5011-1 (Fig. 1) was investigated using initial nondestructive scanning and logging technologies along with multiproxy investigations on subsamples (supplementary materials). The core chronology is based on magnetostratigraphy and tuning of proxy data with marine isotope stratigraphy (*21*) and summer insolation at 67.5°N (*30*) (supplementary materials and figs. S4 and S5).

The sedimentology is composed of five pelagic facies (Fig. 2D; supplementary materials and figs. S1 and S2). One striking feature of the sediments is the remarkably cyclic nature of many proxies, including biogenic silica content (BSi%) and accumulation rate (BSi acc. rate), Si/Ti ratio, and the concentration of total organic carbon (TOC) throughout the record younger than 2.65 Ma (*18*) (Fig. 2, E and F, and fig. S4). BSi percentage and acc. rate and Si/Ti ratios are shown to be robust proxies of the lake's primary productivity, with higher values generally associated with high summer insolation and relatively light marine isotopic values (Fig. 2, A and B). Similar regular cycles are not seen >2.65 Ma. In contrast, high productivity is implied by high Si/Ti ratios and BSi acc. rate from 3.3 to 3.1 Ma (Fig. 2, E and F), but in the early lake history before 3.2 Ma, the productivity signal is diluted by higher clastic flux rates, as evoked by the BSi acc. rate, low Si/Ti ratios, and higher sedimentation rate (Fig. 2E and fig. S3).

Mid-Pliocene Extreme

Our Lake El'gygytgyn record provides a continuous terrestrial record showing the extreme Arctic warmth from 3.6 to 3.4 Ma that other, shorter records of the middle Pliocene have inferred (*31*). The earliest sediment history in the lake begins a few thousand years after the impact, as hydrothermal activity ceased and the crater cooled and filled with water. The first 17 m of post-impact sediment (~the first 20,000 years) is almost devoid of pollen and other microfossils, but after 3.56 Ma, the pollen stratigraphy provides the best descriptor of paleoenvironmental conditions (supplementary materials). The mean temperature of the warmest month (MTWM, Fig. 2H) and PANN (Fig. 2I) reconstructed from the pollen record imply values of +15° to 16°C and ~600 mm/year, respectively. These estimates are 7° to 8°C warmer and 400 mm wetter than today. Similar values were reconstructed for the Pleistocene super-interglacial marine isotope stage (MIS) 11c (*18*), but this time interval lacks fir and hemlock pollen, highlighting the exceptional warmth and wetter conditions of the middle Pliocene. Cooler intervals of the record occur at 3.46 and 3.42 Ma during summer insolation minima and maxima in the marine oxygen isotope stack (e.g., MG6).

Elevated BSi deposition (Fig. 2E) suggests greater seasonal productivity and is consistent with generally warmer and wetter conditions between 3.56 and 3.4 Ma. The dominant planktonic diatom (*Pliocaenicus* sp.) is significantly larger there than during any other interval in the entire lake record, suggesting extremes in nutrient delivery and reduced seasonal ice cover. This is consistent with higher rates of siliciclastic sedimentation, probably caused by increased precipitation, steeper relief, and reduced or absent permafrost within the catchment (supplementary materials, fig. S3).

Mid-Pliocene warmth has previously been documented in other parts of the terrestrial Arctic, but those records are limited in duration, precluding comparisons with orbital forcing. Nonetheless, they provide a vital spatial network of sites for characterizing the Arctic borderlands. The Strathcona Fjord Beaver Pond dated to 3.4 Ma (*32*) (Fig. 1, site 7) spans ~40,000 years. Reconstructed MATs were continuously +19°C warmer than today (–1.6°C), and summer growing season temperatures were in the range of 14°C (*8*, *9*, *32*). The Canadian Archipelago remained a contiguous landmass at this time (*33*) (Fig. 1), with forests likely extending to the coast of the Arctic Ocean (*10*). At the same time, sea surface temperatures (SSTs) in the North Atlantic were 18°C [~7°C warmer than today (Fig. 3D) (*34*)], and latitudinal temperature gradients were lower (*35*, *36*) (Fig. 3H). In Antarctica, persistent open-water conditions in the Ross Embayment and a reduced West Antarctic Ice Sheet from 4.5 to 3.4 Ma imply 1.2 million years of continuous warmth (*37*) (Fig. 3J). Hence, in the mid-Pliocene, both polar regions were substantially warmer than at present. At Lake El'gygytgyn, warm conditions continued even during orbits with reduced boreal summer insolation (Fig. 2, B versus H).

Pliocene-Pleistocene Warmth

Reconstructed MTWM (Fig. 2H) and PANN (Fig. 2I) from 3.26 to 2.2 Ma also indicate a protracted period of warm and moist conditions ~3° to 6°C warmer and <100 to >200 mm wetter than in modern times and warmer than the last interglacial MIS 5e (*18*). Beyond the exceptional vegetation response (Fig. 2, G to I), BSi (Fig. 2E) and TOC (fig. S4) are also elevated during most of this time. Important exceptions to these warm conditions include marine isotopic intervals labeled MIS 100, 96, and 86 (Fig. 2A), when MTWM estimates dip near or below modern values (Fig. 2H) and approach cold temperatures similar to those estimated by the same proxies for late Pleistocene glacial conditions [the Last Glacial Maximum (LGM), Fig. 3A]. Summers cooler than today are largely younger than 2.5 Ma, with only one exception, the M2 cooling event at ~3.3 Ma. Even most early Pleistocene temperatures remained higher than those of the middle and late Pleistocene.

Changes in boreal forest composition occur with the loss of conifers at 2.71 to 2.69 Ma and then the transition from forested habitats to treeless and shrubby environments in steps at 2.6, 2.56, and 2.53 Ma (Fig. 3, G and I). These changes provide estimates of the mean temperature of the coldest month (MTCM; fig. S8), with important implications for Beringian vegetation-climate feedbacks (*38*) as expanding tundra increased land surface albedo, especially during snow-covered months. These cooler vegetation types become dominant <2.53 Ma, even during high summer insolation orbits, except during super-interglacials 93, 91, and 87 (*18*) (supplementary materials). Climate-vegetation model simulations using 300 and 400 ppm CO_2 (Fig. 4 and supplementary materials) are consistent with forest cover at Lake El'gygytgyn before ~2.53 Ma and restricted glacial ice over Greenland in both cold and warm boreal summer orbits (*39*), especially for the PRISM interval from 3.26 to 3.02 Ma (*6*).

Cross-correlation of MTWM (Fig. 3A) with the LR04 stack (Fig. 3B) provides a rather good fit [correlation coefficient (R^2) = 0.41, fig. S8], illustrating the expected link between summer temperatures at Lake El'gygytgyn and obliquity via the isotopic stack (Fig. 3C). Several intervals

of coniferous-dominated forests occurred during MIS 101, 93, 91, and 87 interglacials (*40*). Summers at Lake El'gygytgyn remain 1° to 3°C warmer than at present for ~200,000 years after stratification of the North Pacific at 2.73 Ma (*41*) (Fig. 3F), even during the coldest boreal summer orbits (MIS G6, Fig. 2H). These data, along with eustatic sea-level reconstructions (Fig. 3E), support the notion that Pleistocene cooling and the intensification of Northern Hemisphere glaciation (NHG) were gradual, occurring in several steps (*5*, *34*–*36*), but with warm Arctic

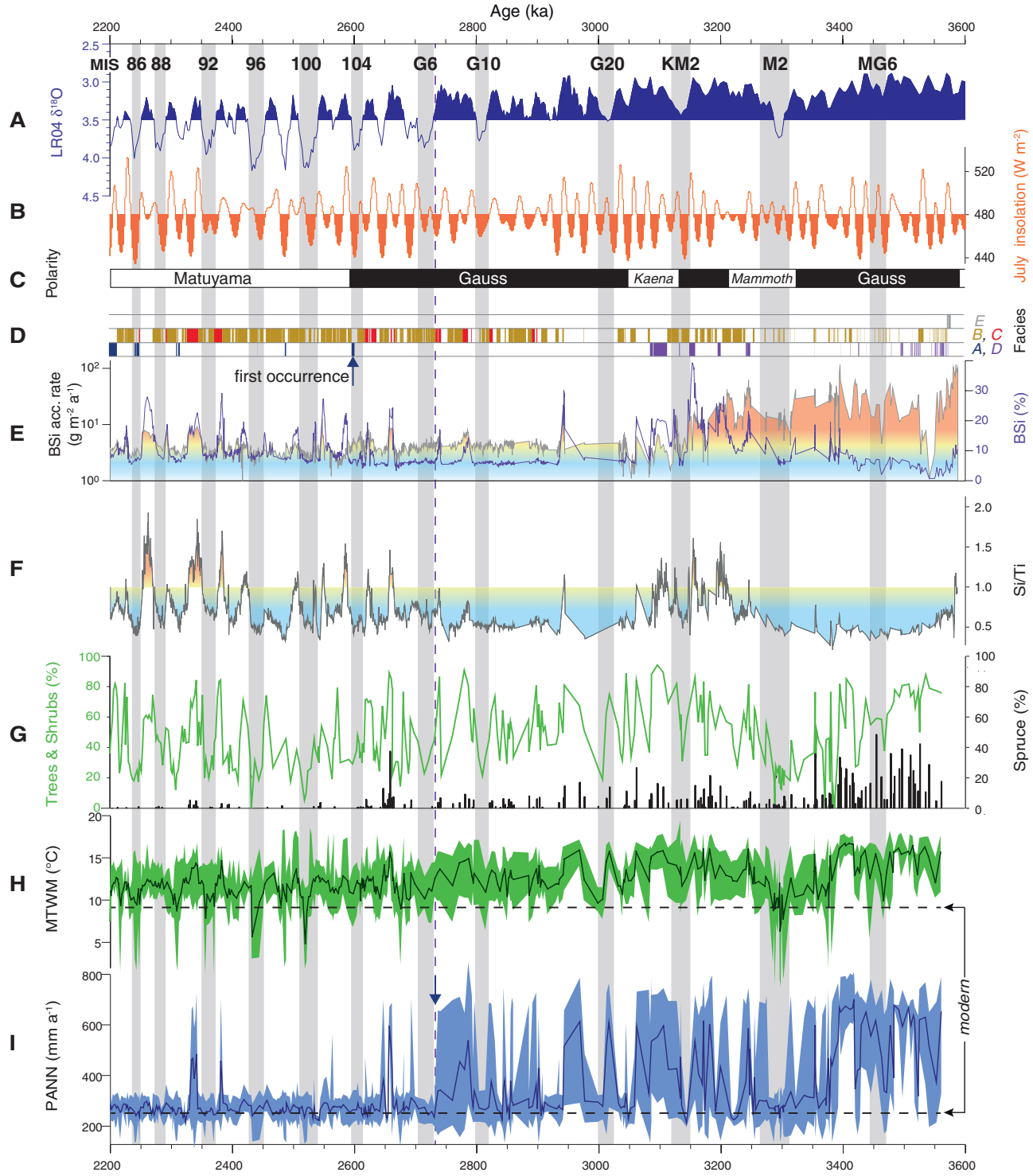

Fig. 2. Chronology, sediment facies, and proxy data from 3.58 to 2.2 Ma from Lake El'gygytgyn. (**A**) Global marine isotope stack (*21*) (ka, thousand years ago) and (**B**) mean July insolation for 67.5°N (*30*), next to (**C**) the magnetostratigraphy, (**D**) sediment facies defined in the text and supplementary materials, (**E**) FTIRS-inferred biogenic silica plotted as BSi acc. rate (note logarithmic scale) and % BSi, and (**F**) Si/Ti ratio. These data are compared to (**G**) percent of trees and shrubs (green line) and spruce (black bars) pollen. (**H**) Reconstructed MTWM and (**I**) annual precipitation (PANN), based on the pollen spectra and the best modern analog approach applied in (*18*). The darker colored line in both (H) and (I) represents the mean values, whereas colored shading is the uncertainty range [modern values from (*63*)].

summers persisting much later than previously documented.

At Lake El'gygytgyn, the PRISM interval (Fig. 3) was nearly as warm as it was between 3.56 and 3.4 Ma, and boreal forests changed little in composition (Fig. 3G). At Meighen Island (Fig. 1, site 6), fossil plant and beetle assemblages suggest July temperatures +10° to 11°C warmer than today (*42*). Data from several sites show that boreal forests stretching from 60° to 80°N included pine, not found in modern forests of Alaska or the Yukon (*31*). Yet the average MTWM reconstructed over the PRISM interval is slightly warmer (~1.5°C) than in multimodel climate simulations of the Pliocene Model Intercomparison Project (PlioMIP) (*43*). In the PlioMIP simulations using eight different coupled atmosphere-ocean general circula-

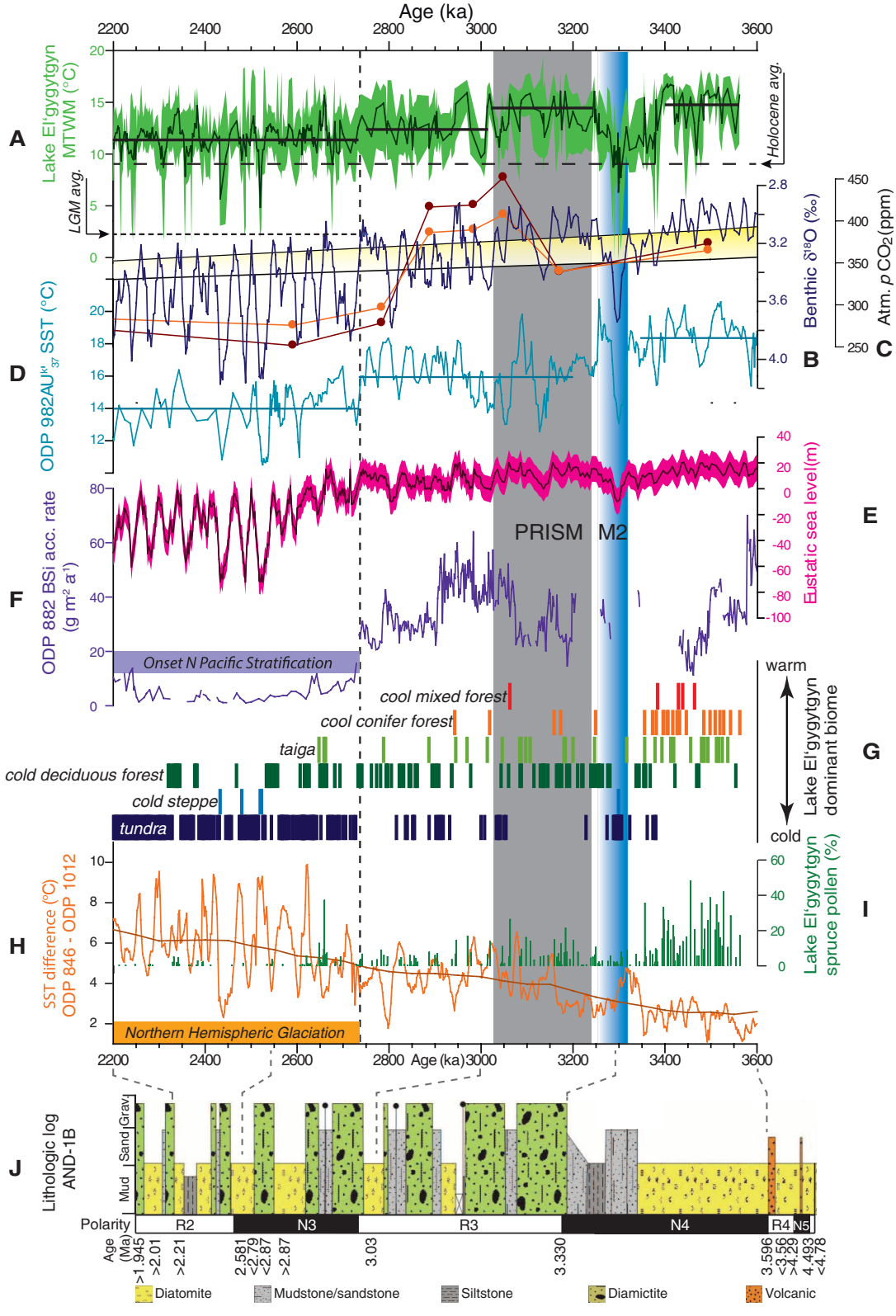

Fig. 3. Global proxies of change compared to Lake El'gygytgyn. (**A**) MTWM from Fig. 2, with solid horizontal lines shown as mean values over the selected intervals; the long dashed line is the Holocene average temperature, and the short dashed line is the LGM average temperature from (*18*). (**B**) Benthic marine LR04 stack (*21*); (**C**) changes in *p*CO2 shown as a range window in yellow, estimated from minimum and maximum of (*2*), with low-resolution estimates using boron methods (orange and red solid circles) in (*3*); (**D**) alkenone reconstructed SSTs for the North Atlantic (*34*) (ODP, Ocean Drilling Program); (**E**) eustatic sea-level record from New Zealand, representative of the global stack (*55*); (**F**) mass accumulation rate of biogenic silica from the North Pacific (*41*); (**G**) dominant reconstructed biomes from Lake El'gygytgyn; (**H**) change in SST gradient between the North Pacific tropics and subtropics from (*59*); (**I**) percent of spruce pollen; compared with (**J**) lithology of ANDRILL core ANT-1B from a depth of 438 to 190 m in (*37*). The blue vertical shading is the M2 isotopic event, and the gray vertical bar is the PRISM research interval. The dashed vertical line marks 2.72 Ma.

tion models (*43*), the multimodel MAT at Lake El′gygytgyn is +7.05° ± 2.7°C warmer than in preindustrial times and the MTWM is 5.5° ± 2°C warmer. The simulated MTWM is close to the PRISM-average reconstructed warming of ~7°C. However, at times during PRISM, MTWM temperatures at the lake were >8°C (Fig. 3A) warmer than present. In sum, model sensitivity to Pliocene boundary conditions, including atmospheric CO_2, appears to be slightly lower than the observed sensitivity at Lake El'gygytgyn.

M2, Pliocene Transition, and Pace of Pleistocene Cooling

The pollen-based reconstructions from Lake El'gygytgyn show that the largest cooling event of the mid-Pliocene took place from 3.31 to 3.28 Ma (MIS M2) (*21*). Conditions were cooler and dryer, as documented by a dramatic decrease in the relative abundance of arboreal pollen and increases in *Artemisia,* Poaceae, and other herbaceous pollen (fig. S6). Although larch, pine, birch, alder, and possibly spruce stands remained around the lake, steppelike habitats dominated (Fig. 3G). Coprophilous fungi indirectly point to the presence of large grazing animals, such as mammoth, horse, and bison (*40*). Climatic conditions were not "glacial"; rather, it was as warm as the Holocene average or slightly warmer (*44*) (Fig. 3A). This has implications for interpreting the M2 isotopic shift of ~0.5 per mil in the North Atlantic (*21*). Modeling sensitivity studies (*39*) do not preclude the existence of a Greenland Ice Sheet during M2 as a major source of ice-rafted debris (IRD) (*45*). However, if Holocene-like conditions at Lake El'gygytgyn are indicative of broader circum-Arctic climate, conditions for the initiation of ice over North America would have been unfavorable until long after 3 Ma (*46*). Our results are consistent with gradual alkenone-based evidence of SST cooling in the eastern North Atlantic in the range of 2° to 3°C (*47*) and 6°C (*34*) during M2, but with ocean temperatures remaining warmer than modern ones both before and after (Fig. 3D). Our findings are also consistent with drilling results from the Ross Sea (ANDRILL), suggesting that most M2 ice advance outside Alaska, Greenland, and Svalbard took place in Antarctica rather than North America (Fig. 3J) (*4*, *37*, *48*).

The gradual but paced onset of NHG took place as step changes starting after 3.6 Ma (*49*), but temperatures in the Arctic remained elevated until ~2.2 Ma. Although records of IRD from the North Atlantic/Barents Sea (*50*) and the North Pacific (*41*) indicate the presence of glacial margins reaching tidewater, IRD records do not provide a measure of ice-sheet size. Eustatic-equivalent changes in sea level, in contrast, offer an index of global ice volume (*21*) but not where the ice was located (*51*).

Direct evidence of North American continental-scale ice sheets extending southward from Canada does not appear until after 2.4 Ma (*52*, *53*) and may have had a different geography with warm-based, subglacial conditions (*54*). This may explain why sea-level variability during initial cold cycles after 2.6 Ma (MIS 100) was in the range of ~70 m, which is much less than ~125 m for the LGM (Fig. 3E) (*55*). In the Alaskan Brooks Range, the earliest glacial cycles were after 2.7 Ma and were most extensive toward the Arctic Ocean,

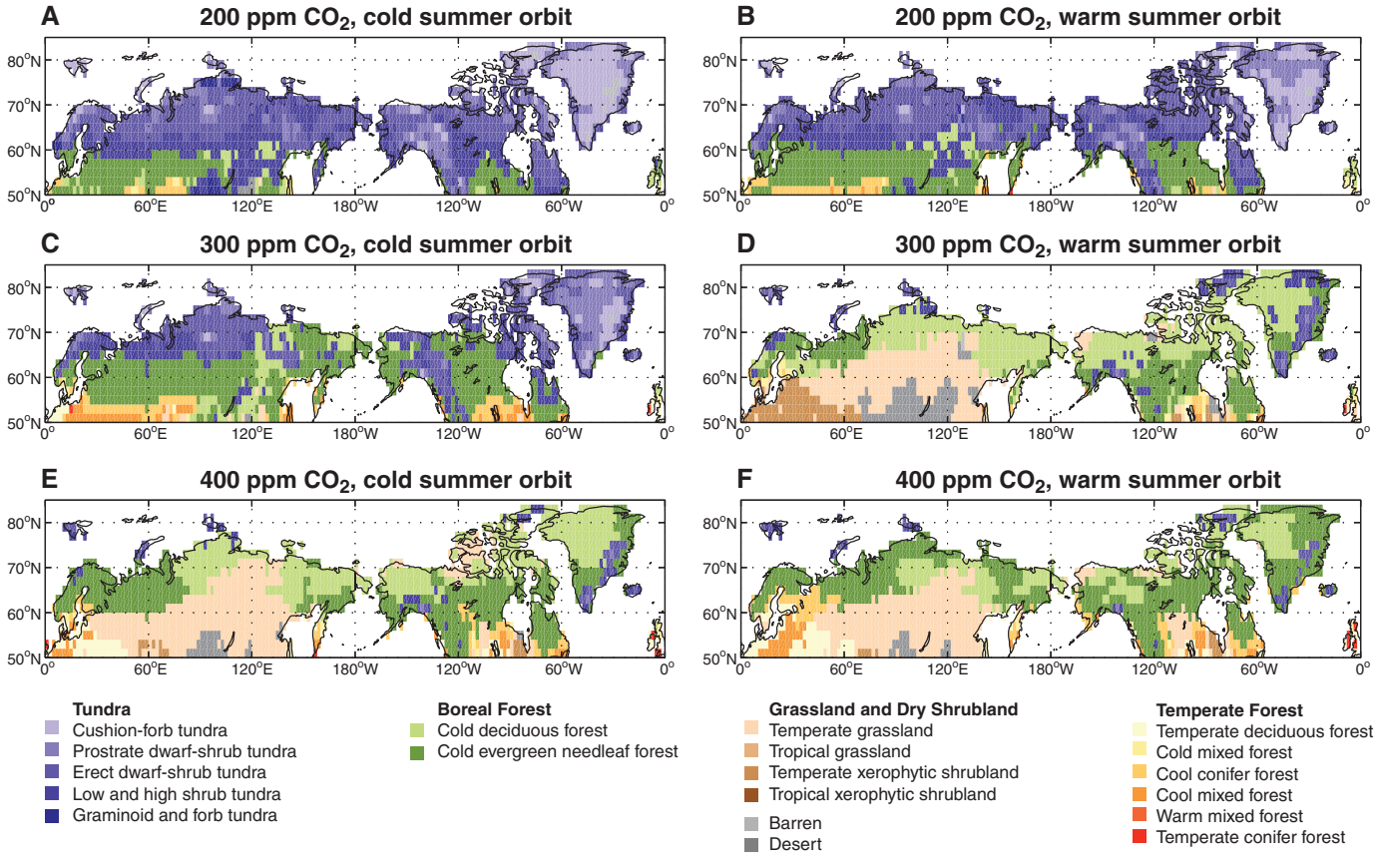

Fig. 4. Coupled climate-vegetation model simulations spanning the Pliocene-Pleistocene transition. All simulations assume an ice-free Northern Hemisphere, including Greenland. CO_2 atmospheric mixing ratios span the range assumed to have existed at the onset of major Pleistocene glacials [**A** and **B**; 200 ppm by volume (ppmv)], during the Pliocene-Pleistocene transition (**C** and **D**; 300 ppmv), and in the warm Pliocene (**E** and **F**; 400 ppmv). (A), (C), and (E) assume an orbital configuration like that at 116 ka, producing relatively cold boreal summers, whereas (B), (D), and (F) use a warm boreal summer orbit like that at 125 ka. The simulations place the pollen-based vegetation reconstruction (Fig. 3G) into a spatial and temporal context, relative to proxy-based CO_2 reconstructions. Although the persistent dominance of forest biomes at Lake El'gygytgyn until 2.6 Ma is in broad agreement with the model, the lack of temperate forest at 400 ppm of CO_2 demonstrates either the undersensitivity of the model to CO_2 forcing or the possibility that Pliocene greenhouse gas levels were higher than in most proxy reconstructions. Descriptions of the model and boundary conditions are provided in the supplementary materials.

suggesting that a more sea-ice–free Arctic Ocean may have provided an important precipitation source (*56*). A major drop in the partial pressure of CO_2 (pCO_2) at ~2.8 Ma that could have driven additional cooling is indicated in some proxy records (*3*) (Fig. 3C). Increases in ocean stratification and IRD in the North Pacific from the mountainous Pacific Rim at 2.73 Ma (*57*), when inferred pCO_2 is in the range of 280 to 370 ppm (*2*, *3*) (Fig. 3C), coincide with a significant drop in precipitation at Lake El'gygytgyn (Fig. 2I) and an abrupt change in boreal forest composition, characterized by vegetation still requiring summer temperatures warmer than the Holocene average (Fig. 3A). Thus, our vegetation record is consistent with estimates for pCO_2 (*2*, *3*), but Arctic temperatures consistent with that vegetation make it difficult to reconcile the buildup of major continental ice sheets with summers warmer than today, even during cold Arctic summer orbits. The substantial PANN drop at 2.73 Ma (Fig. 2I) and onset of cold winter temperatures, at times colder than today (fig. S8), are consistent with preliminary model simulations showing the climatic impact of large Northern Hemispheric ice sheets on the Arctic basin and Beringia (fig. S9).

At Lake El'gygytgyn, the first cold "glacial" sediment, Facies A (Fig. 2D), occurs at ~2.6 Ma (*18*); this facies, indicative of perennial summer lake-ice cover and MAT at least 4° ± 0.5°C colder than today (*58*), becomes common after 2.3 Ma during cooler summer orbits, after an increase in low latitudinal temperature gradients in the Pacific (Fig. 3H) (*59*). Perennial lake-ice cover implied by Facies A does not appear during all cold orbits until after 1.8 Ma (*18*). Likewise, the first cold interval in Lake Baikal occurs at 2.7 Ma, but cyclic patterns of glacial/interglacial BSi do not take hold until after about 1.8 Ma (*36*, *60*).

Warm temperatures and changing boreal forest composition at Lake El'gygytgyn, together with other proxies, contribute to a growing body of marine and terrestrial evidence that climate system change from the warm Pliocene to the late Pleistocene glacial world was a punctuated sequence of stepped Northern Hemispheric cooling events and ice buildup (*34*, *36*, *49*, *59*). Although latitudinal temperature gradients steepened after 2.65 Ma (Fig. 3H), swings in global sea level increase only after 2.6 Ma (Fig. 3E), despite warmer Arctic summers, which is consistent with the waxing and waning of the West Antarctic Ice Sheet (Fig. 3J) (*37*). Polar amplification throughout the interval from 3.56 to 2.2 Ma makes it likely that seasonal rather than perennial Arctic sea ice (*5*) was the norm, particularly during warm summer orbits [(*61*) and supplementary materials].

Conclusions

The sediments recovered at Lake El'gygytgyn provide an exceptional window into environmental dynamics from a terrestrial high-latitude site against which other Arctic and lower-latitude paleoenvironmental records can be compared. Although the geologic record has already informed us of extreme warmth at intervals in the middle Pliocene [(*31*) and references therein], Lake El'gygytgyn provides a continuous time series of the timing of changes responsible for transforming a virtually ice-free forested Arctic into one capable of supporting major glacial cycles. Elevated warmth across cold and warm orbital cycles during the "41,000-year obliquity-dominated world" of the Pliocene and early Pleistocene is consistent with pCO_2 estimates of 280 to 400 ppm (*2*, *3*, *62*), but evidence of extreme polar amplification exceeds that simulated by many climate models. Mechanistic explanations for observed trends in temperature and precipitation have yet to be determined, but imply high sensitivity to CO_2 forcing. The delay of summer cooling in the terrestrial Arctic provides new constraints on Arctic climate and glacial evolution during the onset of NHG.

References and Notes

1. J. Christensen *et al.*, *Fourth Assessment Report of the Intergovernmental Panel on Climate Change* (Cambridge Univ. Press, Cambridge, 2007), pp. 847–940.
2. M. Pagani, Z. Liu, J. LaRiviere, A. C. Ravelo, *Nat. Geosci.* **3**, 27 (2009).
3. O. Seki *et al.*, *Earth Planet. Sci. Lett.* **292**, 201 (2010).
4. T. Naish *et al.*, *Nature* **458**, 322 (2009).
5. J. Matthiessen, J. Knies, C. Vogt, R. Stein, *Philos. Trans. R. Soc. London Ser. A* **367**, 21 (2009).
6. H. J. Dowsett *et al.*, *Stratigraphy* **7**, 123 (2010).
7. International Commission on Stratigraphy, www.stratigraphy.org.
8. A. Z. Csank *et al.*, *Earth Planet. Sci. Lett.* **304**, 291 (2011).
9. A. P. Ballantyne *et al.*, *Geology* **38**, 603 (2010).
10. C. Schweger, D. G. Froese, J. M. White, J. A. Westgate, *Quat. Sci. Rev.* **30**, 2124 (2011).
11. D.A. Darby, *Paleoceanography* **23**, PA1S07 (2008).
12. K. St. John, *Paleoceanography* **23**, PA1S05 (2008).
13. C. E. Stickley *et al.*, *Nature* **460**, 376 (2009).
14. R. Stein, K. Fahl, J. Müller, *Polarforschung* **82**, 37 (2012).
15. M. O'Regan, C. J. Williams, K. E. Frey, M. Jakobsson, *Oceanography* **24**, 66 (2011).
16. L. Polyak *et al.*, *Quat. Sci. Rev.* **29**, 1757 (2010).
17. P. Layer, *Meteorit. Planet. Sci.* **35**, 591 (2000).
18. M. Melles *et al.*, *Science* **337**, 315 (2012).
19. A. S. Studer *et al.*, *Earth Planet. Sci. Lett.* **351-352**, 84 (2012).
20. A. J. Hidy, J. C. Gosse, D. G. Froese, J. D. Bond, D. H. Hood, *Quat. Sci. Rev.* **61**, 77 (2013).
21. L. E. Lisecki, M. E. Raymo, *Paleoceanography* **20**, PA1003 (2005).
22. G. H. Miller *et al.*, *Quat. Sci. Rev.* **29**, 1679 (2010).
23. R. M. Deconto *et al.*, *Nature* **455**, 652 (2008).
24. D. G. Froese, R. W. Barendregt, R. J. Enkin, J. Baker, *Can. J. Earth Sci.* **37**, 863 (2000).
25. M. Nolan, J. Brigham-Grette, *J. Paleolimnol.* **37**, 17 (2007).
26. O. Y. Glushkova, V. N. Smirnov, *J. Paleolimnol.* **37**, 37 (2007).
27. O. Juschus, F. Preusser, M. Melles, U. Radtke, *Quat. Geochronol.* **2**, 187 (2007).
28. M. Melles *et al.*, *Sci. Drill.* **11**, 29 (2011).
29. A. C. Gebhardt, F. Niessen, C. Kopsch, *Geology* **34**, 145 (2006).
30. J. Laskar *et al.*, *Astron. Astrophys.* **428**, 261 (2004).
31. J. V. Matthews Jr., A. Telka, in *Insects of the Yukon*, H. V. Danks, J. A. Downes, Eds. [Biological Survey of Canada (Terrestrial Arthropods), Ottawa, Canada, 1997] pp. 911–962.
32. N. Rybczynski *et al.*, *Nat. Commun.* **4**, 1550 (2013).
33. J. England, *Geology* **15**, 419 (1987).
34. K. T. Lawrence, T. D. Herbert, C. M. Brown, M. E. Raymo, A. M. Haywood, *Paleoceanography* **24**, PA2218 (2009).
35. C. M. Brierley, A. V. Federov, *Paleoceanography* **25**, PA2214 (2010).
36. T. D. Herbert, L. C. Peterson, K. T. Lawrence, Z. Liu, *Science* **328**, 1530 (2010).
37. R. McKay *et al.*, *Proc. Natl. Acad. Sci. U.S.A.* **109**, 6423 (2012).
38. S. Levis, J. A. Foley, D. Pollard, *Geophys. Res. Lett.* **26**, 747 (1999).
39. S. J. Koenig, R. M. DeConto, D. Pollard, *Clim. Dyn.* **37**, 1247 (2011).
40. A. A. Andreev *et al.*, Late Pliocene/Early Pleistocene environments of the north-eastern Siberia inferred from Lake El'gygytgyn pollen record. 12th International Paleolimnology Symposium, Glasgow, Scotland, 21 to 24 August 2012, p. 197.
41. G. H. Haug *et al.*, *Nature* **433**, 821 (2005).
42. S. A. Elias, J. V. Matthews Jr., *Can. J. Earth Sci.* **39**, 911 (2002).
43. A. M. Haywood *et al.*, *Clim. Past* **8**, 2969 (2012).
44. D. S. Kaufman *et al.*, *Quat. Sci. Rev.* **23**, 529 (2004).
45. E. Jansen, T. Fronval, F. Rack, J. E. T. Channell, *Paleoceanography* **15**, 709 (2000).
46. G. S. Dwyer, M. A. Chandler, *Philos. Trans. A Math. Phys. Eng. Sci.* **367**, 157 (2009).
47. S. De Schepper, M. J. Head, J. Groeneveld, *Paleoceanography* **24**, PA4206 (2009).
48. D. Pollard, R. M. DeConto, *Nature* **458**, 329 (2009).
49. K. T. Lawrence, S. Sosdian, H. E. White, Y. Rosenthal, *Earth Planet. Sci. Lett.* **300**, 329 (2010).
50. J. Knies *et al.*, *Quat. Sci. Rev.* **28**, 812 (2009).
51. M. E. Raymo, J. X. Mitrovica, M. J. O'Leary, R. M. DeConto, P. J. Hearty, *Nat. Geosci.* **4**, 328 (2011).
52. A. Duk-Rodkin, R. W. Barendregt, J. M. White, *Can. J. Earth Sci.* **47**, 1003 (2010).
53. G. Balco, C. W. Rovey, *Geology* **38**, 795 (2010).
54. P. U. Clark, D. Pollard, *Paleooceanography* **13**, 1 (1998).
55. K. G. Miller *et al.*, *Geology* **40**, 407 (2012).
56. T. D. Hamilton, K. Reed, R. Thorson, *Glaciation in Alaska: The Geologic Record* (Alaska Geological Society, Anchorage, AK, 1986).
57. K. Takahashi *et al.*, *Sci. Drill.* **11**, 4 (2011).
58. M. Nolan, *Clim. Past Disc* **8**, 1443 (2012).
59. C. M. Brierley *et al.*, *Science* **323**, 1714 (2009).
60. A. Prokopenko *et al.*, *Quat. Int.* **80-81**, 37 (2001).
61. J. Brigham-Grette, L. D. Carter, *Arctic* **43**, 74 (1992).
62. G. Bartoli, B. Hönisch, R. E. Zeebe, *Paleoceanography* **26**, PA4213 (2011).
63. M. New, D. Lister, M. Hulme, I. Makin, *Clim. Res.* **21**, 1 (2002).

Acknowledgments: Drilling operations were funded by the ICDP, the U.S. National Science Foundation (NSF), the German Federal Ministry of Education and Research (BMBF), the Alfred Wegener Institute and Helmholtz Centre Potsdam, the Far East Branch of the Russian Academy of Sciences, the Russian Foundation for Basic Research, and the Austrian Federal Ministry of Science and Research (BMWF). The Russian GLAD 800 drilling system was developed and operated by DOSECC Inc. We thank all participants of the expedition for their engagement during the recovery of the ICDP 5011-1 cores. Funding of core analyses was provided by BMBF (grant no. 03G0642), the German Research Foundation (DFG, grant nos. ME 1169/21 and ME 1169/24), NSF (grant no. 0602471), the Global Civilian Research and Development Foundation (CGP-RFBR IV, grant no. RUG1-2987-MA-10), Vetenskapsrådet, the Swedish Research Council Formas, and the Kempe Foundation. P.T. acknowledges DFG Heisenberg Program (grant no. TA 540/5). We are grateful to N. Mantke,

A. Shahnazarian, and various students (Univ. of Cologne) for their help in core processing and to T. Matrosova for contributing modern surface pollen data. Thanks to A. Dolan for supplying PlioMIP model output and I. Castañeda for discussions and help with figures. The data reported in this paper are archived in the databases of PANGAEA (doi:10.1594/PANGAEA.808834) and the U.S. National Geophysical Data Center (ftp://ftp.ncdc.noaa.gov/pub/data/paleo/paleolimnology/asia/russia/elgygytgyn2013.xls).

Supplementary Materials
www.sciencemag.org/cgi/content/full/science.1233137/DC1
Materials and Methods
Supplementary Text
Figs. S1 to S9
Tables S1 to S5
References (*64*–*105*)

23 November 2012; accepted 24 April 2013
Published online 9 May 2013;
10.1126/science.1233137

Massive Dirac Fermions and Hofstadter Butterfly in a van der Waals Heterostructure

B. Hunt,[1]* J. D. Sanchez-Yamagishi,[1]* A. F. Young,[1]* M. Yankowitz,[2] B. J. LeRoy,[2] K. Watanabe,[3] T. Taniguchi,[3] P. Moon,[4]† M. Koshino,[4] P. Jarillo-Herrero,[1]‡ R. C. Ashoori[1]‡

van der Waals heterostructures constitute a new class of artificial materials formed by stacking atomically thin planar crystals. We demonstrated band structure engineering in a van der Waals heterostructure composed of a monolayer graphene flake coupled to a rotationally aligned hexagonal boron nitride substrate. The spatially varying interlayer atomic registry results in both a local breaking of the carbon sublattice symmetry and a long-range moiré superlattice potential in the graphene. In our samples, this interplay between short- and long-wavelength effects resulted in a band structure described by isolated superlattice minibands and an unexpectedly large band gap at charge neutrality. This picture is confirmed by our observation of fractional quantum Hall states at $\pm^5/_3$ filling and features associated with the Hofstadter butterfly at ultrahigh magnetic fields.

The ability to tailor the properties of electronic devices is one of the landmark achievements of modern technology and motivates a sizable fraction of modern research in condensed matter physics. Just as crystal structure can determine the electronic properties of a material, artificial periodic superstructures can be used to modify the electronic band structure of existing materials (*1*). The band structure of pristine graphene consists of linearly dispersing energy bands, which touch at two degenerate "Dirac points." This degeneracy is protected by the equivalence of the A and B triangular sublattices that make up the graphene honeycomb (*2*) and is responsible for graphene's semimetallic behavior. Theory suggests that the electronic properties of graphene can be tuned via external periodic potentials: Long-wavelength superlattices have been predicted to lead to the formation of additional gapless Dirac points at finite energy (*3*), whereas atomic-scale modulations, by breaking the A-B sublattice symmetry, may turn graphene from a semimetal into a semiconductor (*4*). Experimental efforts to make high-mobility functional devices based on band structure engineering, however, have been hindered by growth and nanofabrication limitations (*5*).

Recently, a new approach has become available through the use of hexagonal boron nitride (hBN) as a planar crystalline substrate. hBN is isostructural to graphene but has boron and nitrogen atoms on the A and B sublattices, leading to a large band gap (*6*). The weak interlayer van der Waals forces in both graphene and hBN permit the fabrication of multilayer heterostructures by sequential transfer of individual layers (*7*). During the transfer process, the angular alignment of the constituent crystals (θ) can in principle be controlled, but the graphene and hBN lattices retain their natural 1.8% mismatch (*4*). The frequency difference of the mismatched lattices leads to the formation of a moiré pattern with wavelength λ(θ) that can be much larger than the lattice constant (*8*, *9*) (Fig. 1A).

The effect of the moiré on the graphene electronic structure can be decomposed into two parts (*10*). The moiré pattern results in a λ-scale modulation of the graphene-hBN coupling, forming a smooth superlattice potential. More subtly, the moiré also modulates the local asymmetry

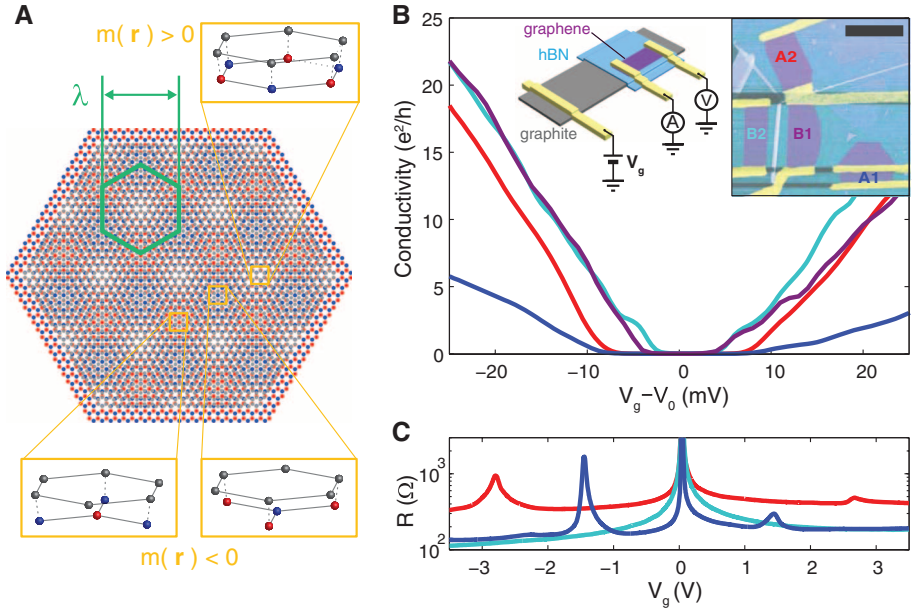

Fig. 1. Insulating states and superlattice minibands in a graphene-hBN heterostructure. (A) Schematic of the moiré pattern for graphene (gray) on hBN (red and blue), for zero misalignment angle and an exaggerated lattice mismatch of ~10%. The moiré unit cell is outlined in green. Regions of local quasi-epitaxial alignment lead to opposite signs of the sublattice asymmetry, $m(\mathbf{r})$, in different regions (gray, carbon; red, boron; blue, nitrogen). **(B)** Low-temperature (T = 150 mK) conductivity near charge neutrality of four heterostructure devices (A1, A2, B1, and B2). The CNP offset V_0 = 37, 37, 46, and 42 mV, respectively. Left inset: Measurement schematic. Right inset: False-color atomic force microscopy image. Scale bar, 3 μm. **(C)** Resistance over a larger gate range. Finite-density resistance peaks indicate full filling of the lowest superlattice miniband in two of the four measured devices (A1 and A2) within the experimentally accessible density range.

[1]Department of Physics, Massachusetts Institute of Technology, Cambridge, MA 02139, USA. [2]Department of Physics, University of Arizona, Tucson, AZ 85721, USA. [3]Advanced Materials Laboratory, National Institute for Materials Science, Tsukuba, Ibaraki 305-0044, Japan. [4]Department of Physics, Tohoku University, Sendai 980-8578, Japan.

*These authors contributed equally to this work.
†Present address: Korea Institute for Advanced Study, Seoul 130-722, Republic of Korea.
‡Corresponding author. E-mail: pjarillo@mit.edu (P.J.-H.); ashoori@mit.edu (R.C.A.)